Hindawi Publishing Corporation
Advances in Astronomy
Volume 2010, Article ID 768675, 15 pages
doi:10.1155/2010/768675

Review Article

Non-Gaussianity from Large-Scale Structure Surveys

Licia Verde

Institució Catalana de Recerca i Estudis Avançat (ICREA) & Instituto de Ciencias del Cosmos, Universitat de Barcelona-IEEC (ICC-UB), Marti i Franques 1, 08028 Barcelona, Spain

Correspondence should be addressed to Licia Verde, liciaverde@icc.ub.edu

Received 27 January 2010; Accepted 18 March 2010

Academic Editor: Dragan Huterer

With the advent of galaxy surveys which provide large samples of galaxies or galaxy clusters over a volume comparable to the horizon size (SDSS-III, HETDEX, Euclid, JDEM, LSST, Pan-STARRS, CIP, etc.) or mass-selected large cluster samples over a large fraction of the extra-galactic sky (Planck, SPT, ACT, CMBPol, B-Pol), it is timely to investigate what constraints these surveys can impose on primordial non-Gaussianity. I illustrate here three different approaches: higher-order correlations of the three dimensional galaxy distribution, abundance of rare objects (extrema of the density distribution), and the large-scale clustering of halos (peaks of the density distribution). Each of these avenues has its own advantages, but, more importantly, these approaches are highly complementary under many respects.

1. Introduction

The recent advances in the understanding of the origin and evolution of the Universe have been driven by the advent of high-quality data, in unprecedented amount (just think of WMAP and SDSS, e.g.). Despite this, most of the information about cosmological parameters come from the analysis of a massive compression of the data: the power spectrum of their statistical fluctuations over the mean. The power spectrum is a complete statistical description of a random field only if it is Gaussian.

Even the simplest inflationary models predict deviations from Gaussian initial conditions. These deviations are expected to be small, although "small" in some models may be "detectable." For a thorough review of inflationary non-Gaussianity see [1]; for our purpose it will be sufficient to say that to describe inflation-motivated departures from Gaussian initial conditions many write [2–5]

$$\Phi = \phi + f_{\rm NL}(\phi^2 - \langle\phi^2\rangle). \tag{1}$$

Here ϕ denotes a gaussian field and Φ denotes Bardeen's gauge-invariant potential, which, on sub-Hubble scales reduces to the usual Newtonian peculiar gravitational potential, up to a minus sign. In the literature, there are two conventions for (1): the large-scale structure (LSS) and the Cosmic Microwave Background (CMB) one. In the LSS convention Φ is linearly extrapolated at $z = 0$; in the CMB convention Φ is instead primordial: thus $f_{\rm NL}^{\rm LSS} = g(z = \infty)/g(0) f_{\rm NL}^{\rm CMB} \sim 1.3 f_{\rm NL}^{\rm CMB}$, where $g(z)$ denotes the linear growth suppression factor relative to an Einstein-de-Sitter Universes. In the past few years it has become customary to always report $f_{\rm NL}^{\rm CMB}$ values even if, for simplicity as it will be clear below, one carries out the calculations with $f_{\rm NL}^{\rm LSS}$.

While for simplicity one may just assume $f_{\rm NL}$ in (1) to be a constant (yielding the so-called *local* model or *local*-type) in reality the expression is more complicated and $f_{\rm NL}$ is scale and configuration dependent. Even if the bispectrum does not completely specify non-Gaussianity, in most practical applications, the non-Gaussianity is set by writing down the bispectrum of Φ. For example, one can see that for the local model the bispectrum is

$$B_\Phi(k_1, k_2, k_3) = 2 f_{\rm NL} P_\phi(k_1) P_\phi(k_2) + 2 \text{ cyc}, \tag{2}$$

where P denotes the power spectrum and it is often assumed that $P_\phi = P_\Phi$; "cyc." denotes two cyclic terms over k_1, k_2, k_3.

It has been shown [6] that for non-Gaussianity of the local type the bispectrum is dominated by the so-called *squeezed* configurations, triangles where one wave-vector length is much smaller than the other two. Models such as the curvaton for example, have a non-Gaussianity of the local type. Standard, single-field slow roll inflation also yields a local non-Gaussianity but with an unmeasurably small $f_{\rm NL}$ (see [1] and references therein). On the other hand, many inflationary models have an *equilateral*-type non-Gaussianity, that is, the bispectrum is dominated by equilateral triangles [6]. References [7, 8] have proposed a functional form which closely approximates the behavior of the inflationary bispectrum and which is useful for efficient data-analysis:

$$\begin{aligned} B(k_1,k_2,k_3) = 6f_{\rm NL}\Big\{ & -P(k_1)P(k_2) + 2\text{cyc.} \\ & -2[P(k_1)P(k_2)P(k_3)]^{2/3} \\ & +P^{1/3}(k_1)P^{2/3}(k_2)P(k_3) + 5\text{cyc.}\Big\}. \end{aligned} \tag{3}$$

Note that the same numerical value for $f_{\rm NL}$ gives rise to a larger skewness in the local case than in the equilateral case (e.g., see [9]), explaining why the CMB constraints on $f_{\rm NL}$ are weaker for the equilateral case [7, 8, 10].

Specific deviations from a single field, slow roll, canonical kinetic energy, Bunch-Davies vacuum, leave their specific signature on the bispectrum "shape" (i.e., the dependence of B on the shape of the triangle made by the three $\vec{k}$ vectors), see discussion in [11] and references therein.

Non-Gaussianity therefore offers a probe of aspects of inflation (namely, the interactions of the inflaton) that are difficult to probe by other means (i.e., measuring the shape of the primordial power spectrum and properties of the stochastic background of gravity waves). So, how could primordial non-Gaussianity be tested?

One could look at the early Universe: by looking at CMB anisotropies we can probe cosmic fluctuations at a time when their statistical distribution should have been close to their original form but the signal is small. On the other hand, one could analyze the statistics of the large-scale structures, close to the present-day, when the overdensities are larger, but this is a more complicated approach, since gravitational instability (for the dark matter distribution) and bias (for galaxies or clusters of galaxies) introduce non-Gaussian features in an initially Gaussian field and they mask the signal one is after. Finally, the abundance of rare events (such as galaxy clusters and high-redshift galaxies) probes the tails of the PDF of the density field, which are extremely sensitive to deviations from Gaussianity. Here, I will concentrate on the signature of non-Gaussianity on large-scale structure (i.e., at redshift $z \lesssim 1$) as they can be traced by galaxy surveys (i.e., I will not consider wide field weak gravitational lensing surveys); other contributions to this review will focus on non-Gaussian signatures on the CMB, thus here it will be sufficient to give only a very brief and succinct introduction to the subject.

At recombination fluctuations are small (recall that $\delta_\Phi \sim 10^{-5}$), and the CMB temperature fluctuations are directly related to Φ making this a very clean probe. However, effectively only one redshift can be tested giving us only a 2-dimensional information.

The most widespread technique for testing Gaussianity in the CMB is to use the CMB bispectrum:

$$\left\langle a_{\ell_1}^{m_1} a_{\ell_2}^{m_2} a_{\ell_3}^{m_3} \right\rangle = B_{\ell_1\ell_2\ell_3} \begin{pmatrix} \ell_1 & \ell_2 & \ell_3 \\ m_1 & m_2 & m_3 \end{pmatrix}, \tag{4}$$

where the a_ℓ^m are the coefficients of the spherical harmonic expansion of the CMB temperature fluctuation: $\Delta T/T = \sum_{\ell m} a_\ell^m Y_\ell^m$ and the presence of the 3-J symbol ensures that the bispectrum is defined if $l_1 + l_2 + l_3 =$ even, $\ell_j + \ell_k \geq l_i \geq |l_j - \ell_k|$ (triangle rule), and that $m_1 + m_2 + m_3 = 0$. It should be however clear that secondary CMB anisotropies and foregrounds also induce a CMB bispectrum which can mask or partially mimic the signal see, for example [5, 12–17] and references therein.

In the last few years, this area of research has received an impulse, motivated by the recent full sky CMB data from WMAP. In particular it has been shown that the constraints can be greatly improved by effectively "reconstructing" the potential Φ from CMB temperature and polarization data rather than simply using the temperature bispectrum alone [18, 19]. This technique would yield constraints on non-Gaussianity of the local type of $\Delta f_{\rm NL} \sim 1$ for an ideal experiment and $\Delta f_{\rm NL} \sim 3$ for the Planck satellite. This is particularly promising as $f_{\rm NL}$ of order unity or larger is produced by broad classes of inflationary models (see e.g., [1] and references therein).

Currently, the most stringent constraints for the local type are $27 < f_{\rm NL} < 147$ at the 95% confidence (central value 87) from WMAP 3 years data [20]; and from the WMAP 5 years data, $-9 < f_{\rm NL} < 111$ at the 95% confidence level (central value 55) [10] and $-4 < f_{\rm NL} < 80$ [21]. Despite the heated debate on whether $f_{\rm NL} = 0$ is ruled out or not, the two measurements are not necessarily in conflict: the two central values differ by only about 1σ; different, although not independent, data sets were used with different galactic cuts, and the maximum multipole considered in the analyses is also different. What makes the subject very interesting, is that, if the central value for $f_{\rm NL}$ is truly around 60, forthcoming data will yield a highly-significant detection.

2. Higher-Order Correlations

Theoretical considerations (see discussion in e.g., [11] and references therein) lead us to define primordial non-Gaussianity by its bispectrum. While in principle there may be types of non-Gaussianity which would be more directly related to higher-order correlations (e.g., [22] and references therein), and while a full description of a non-Gaussian distribution would require the specification of all the higher-order correlations, it is clear that quantities such as the bispectrum enclose information about the phase correlation between k-modes. In the Gaussian case, different Fourier modes are uncorrelated (by definition of Gaussian random phases) and a statistic like the power spectrum does not carry information about phases. The bispectrum is the lowest-order correlation with zero expectation value in a Gaussian random field. But, even if the initial conditions were Gaussian, nonlinear evolution due to gravitational instability generates a nonzero bispectrum. In particular, gravitational instability has its own "signature" bispectrum, at least in the next-to-leading order in cosmological perturbation theory [23]:

$$B\left(\vec{k}_1, \vec{k}_2, \vec{k}_3\right) = 2P(k_1)P(k_2)J\left(\vec{k}_1, \vec{k}_2\right) + 2\text{cyc}, \quad (5)$$

where $J(\vec{k}_1, \vec{k}_2)$ is the gravitational instability "kernel" which depends very weakly on cosmology and for an Einstein-de-Sitter Universe is

$$J\left(\vec{k}_1, \vec{k}_2\right) = \frac{5}{7} + \frac{\vec{k}_1 \cdot \vec{k}_2}{2k_1k_2}\left(\frac{k_1}{k_2} + \frac{k_2}{k_1}\right) + \frac{2}{7}\left(\frac{\vec{k}_1 \cdot \vec{k}_2}{k_1k_2}\right)^2. \quad (6)$$

In the highly nonlinear regime the detailed form of the kernel changes, but it is something that could be computed and calibrated by extending perturbation theory beyond the next-to-leading order and by comparing with numerical N-body simulations (see other contributions in this issue). It was recognized a decade ago [4] that this signal is quite large compared to any expected primordial non-Gaussianity and that the primordial signal "redshifts away" compared to the gravitational signal. In fact, a primordial signal given by a local type of non-Gaussianity parameterized by a given f_{NL}, would affect the late-time dark matter density bispectrum with a contribution of the form

$$\begin{aligned} &B^{f_{\text{NL}}\ \text{local}}\left(\vec{k}_1, \vec{k}_2, \vec{k}_3, z\right) \\ &\quad = 2f_{\text{NL}}P(k_1)P(k_2)\frac{\mathcal{F}\left(\vec{k}_1, \vec{k}_2\right)}{D(z)/D(z=0)} + 2\text{cyc}, \end{aligned} \quad (7)$$

where $D(z)$ is the linear growth function which in an Einstein-de-Sitter universe goes like $(1+z)^{-1}$ and

$$\mathcal{F} = \frac{\mathcal{M}(k_3)}{\mathcal{M}(k_1)\mathcal{M}(k_2)}; \qquad \mathcal{M}(k) = \frac{2}{3}\frac{k^2T(k)}{H_0^2\Omega_{m,0}}, \quad (8)$$

$T(k)$ denoting the transfer function, H_0 the Hubble parameter, and $\Omega_{m,0}$ the matter density parameter. Clearly the two contributions have different scale and redshift dependence and the two kernel shapes in configuration space are different, thus, making the two components, at least in principle and for high signal-to-noise, separable.

Unfortunately, with galaxy surveys, one does not observe the dark matter distribution directly. Dark matter halos are believed to be hosts for galaxy formation, and different galaxies at different redshifts populate halos following different prescriptions. In large-scale structure studies, often the assumption of linear scale independent bias is made. A linear bias will not introduce a nonzero bispectrum in a Gaussian field and its effect on a field with a nonzero bispectrum is only to rescale its bispectrum amplitude. This is, however, an approximation, possibly roughly valid at large scales for dark matter halos, and when looking at the power spectrum, but unlikely to be true in detail. To go beyond the linear bias assumption, often the assumption of quadratic bias is made, where the relation between dark matter overdensity field and galaxy field is specified by two parameters: b_1 and b_2, $\delta_g(x) = b_1\delta_{\text{DM}}(x) + b_2(\delta_{\text{DM}}^2 - \langle\delta_{\text{DM}}^2\rangle)$; b_1 and b_2 are assumed to be scale-independent (although this assumption must break down at some point) but they can vary with redshift. Clearly, a quadratic bias will introduce non-Gaussianity even on an initially Gaussian field. In summary, for local non-Gaussianity and scale-independent quadratic bias we have [4, 24]

$$\begin{aligned} &B\left(\vec{k}_1, \vec{k}_2, \vec{k}_3, z\right) \\ &\quad = 2P(k_1)P(k_2)b_1(z)^3 \\ &\qquad \times \left[f_{\text{NL}}\frac{\mathcal{F}\left(\vec{k}_1, \vec{k}_2\right)}{D(z)} + J\left(\vec{k}_1, \vec{k}_2\right) + \frac{b_2(z)}{2b_1(z)}\right] + \text{cyc}. \end{aligned} \quad (9)$$

Before the above expression can be compared to observations it needs to be further complicated by redshift space distortions (and shot noise). Realistic surveys use the redshift as a proxy for distance, but gravitationally induced peculiar velocities distort the redshift-space galaxy distribution. We will not go into these details here as including redshift space distortions (and shot noise) will not change the gist of the message.

From a practical point of view, it is important to note that photometric surveys, although in general can cover larger volumes that spectroscopic ones, are not suited for this analysis: the projection effects due to the photo-z smearing along the line-of-sight is expected to suppress significantly the sensitivity of the measured bispectrum to the shape of the primordial one (see e.g., [25, 26]).

Reference [4] concluded that "CMB is likely to provide a better probe of such (local) non-Gaussianity." Much more recently, reference [27] revisited the issue and found that, assuming a given known redshift dependence of the (b_1, b_2) bias parameters and an all sky survey from $z = 0$ to $z = 5$ with a galaxy number density of at least $5 \times 10^{-4}\,\text{h}^3/\text{Mpc}^3$, the galaxy bispectrum can provide constraints on the f_{NL} parameter competitive with CMB. However, for all planned surveys, the forecasted errors are much larger than Planck forecasted errors. This holds qualitatively also for the equilateral case.

While the gravitationally induced non-Gaussian signal in the bispectrum has been detected to high statistical significance (see [28] and references therein, see also other contributions to this issue), the nonlinear bias signature is not uncontroversial, and there have been so far no detection of any extra (primordial) bispectrum contributions.

Of course one could also consider higher-order correlations. One of the advantages of considering, for example, the trispectrum is that, contrary to the bispectrum, it has very weak nonlinear growth [29], but has the disadvantage that the signal is delocalized: the number of possible configurations grows fast with the dimensionality n of the n-point function!

In summary, higher-order correlations as observed in the CMB or in the evolved Universe, can be used to determine the bispectrum *shape*. The two approaches should be seen as complementary as they are affected by different systematic effects and probe different scales. The next two probes we consider have a less-rich sensitivity to the bispectrum shape, but their own peculiar advantages.

3. The Mass Function

The abundance of collapsed objects (dark matter halos as traced, e.g., by galaxies and galaxy clusters) contains important information about the properties of initial conditions on galaxy and clusters scales. The Gaussian assumption plays a central role in analytical predictions for the abundance and statistical properties of the first objects to collapse in the Universe. In this context, the formalism proposed by Press and Schechter [30], with its later extensions and improvements, has become the standard lore for predicting the number of collapsed dark matter halos as a function of redshift. However, even a small deviation from Gaussianity can have a deep impact on those statistics which probe the tails of the distribution. This is indeed the case for the abundance of high-redshift objects like galaxies and clusters at $z \gtrsim 1$ which correspond to high peaks, that is, rare events, in the underlying dark matter density field. Therefore, even small deviations from Gaussianity might be potentially detectable by looking at the statistics of high-redshift systems. Before proceeding let us introduce some definitions.

We are interested in predictions for rare objects, that is the collapsed objects that form in extreme peaks of the density field $\delta(x) = \delta\rho/\rho$. The statistics of collapsed objects can be described by the statistics of the density perturbation smoothed on some length scale R (or equivalently a mass scale $M = 4/3\pi R^3\rho$), δ_R.

To incorporate non-Gaussian initial conditions into predictions for the smoothed density field, we need an expression for the probability distribution function (PDF) for δ_R. For a particular real-space expansion like (1), one may make a formal change of variable in the Gaussian PDF to generate a normalized distribution [31]. However, this may not be possible in general and the change of variables does not work for the smoothed cumulants of the density field. In general, the PDF for a generic non-Gaussian distribution can be written exactly as a function of the cumulant's generating function $\mathcal{W}_R$ for the smoothed density field:

$$\mathcal{P}(\delta_R)d\delta_R = \int \frac{d\lambda}{2\pi} \exp[-i\lambda\delta_R + \mathcal{W}_R(\lambda)]d\delta_R \tag{10}$$

with

$$\mathcal{W}_R(\lambda) = \sum_{n=2}^{\infty} \frac{(i\lambda)^n}{n!}\mu_{n,R}, \tag{11}$$

where $\mu_{n,R}$ denote the cumulants and, for example, $\mu_{2,R} = \sigma_R^2 = \langle\delta_R^2\rangle$ and the skewness $\mu_{3,R}$ is related to the normalized skewness of the smoothed density field $S_{3,R} = \mu_{3,R}/\mu_{2,R}^2$. It is useful to define a "skewness per $f_{\rm NL}$ unit" $S_{3,R}^{f_{\rm NL}=1}$ so that $S_{3,R} = f_{\rm NL}S_{3,R}^{f_{\rm NL}=1}$. The skewness $\mu_{3,R}$ is related to the underlying bispectrum by

$$\mu_{3,R} = \int \frac{d^3k_1 d^3k_2 d^3k_3}{(2\pi)^6} B_{\delta,R}\left(\vec{k}_1, \vec{k}_2, \vec{k}_3\right)\delta^D_{\vec{k}_1+\vec{k}_2+\vec{k}_3}, \tag{12}$$

where δ^D denotes the Dirac delta function and $B_{\delta,R}$ denotes the bispectrum of the δ overdensity field smoothed on scale R. It is related to the potential one trivially by remembering the Poisson equation: $\delta_R(\vec{k}) = \mathcal{M}(k)W_R(k)\Phi(\vec{k})$. Here, $W_R(k)$ denotes the smoothing kernel, usually taken to be the Fourier transform of the top hat window. In any practical application the dimensionality of the integration can be reduced by collapsing the expressing $\vec{k}_3$ as a function of $\vec{k}_1$ and $\vec{k}_2$.

It is important at this point to make a small digression to specify definitions of key quantities. Even in linear theory, the normalized skewness of the density field depends on redshift; however in the Press and Schechter framework one should always use linearly extrapolated quantities at $z = 0$. In this context therefore, when writing $S_{3,R} = f_{\rm NL}S_{3,R}^{f_{\rm NL}=1}$, if $S_{3,R}^{f_{\rm NL}=1}$ is that if the density field extrapolated linearly at $z = 0$ then $f_{\rm NL}$ must be the LSS one and not the CMB one.

To compute the abundance of collapsed objects from the PDF one will then follow the Press and Schechter swindle: first compute

$$\mathcal{P}(>\delta_c \mid z, R) = \int_{\delta_c(z)}^{\infty} d\delta_R \mathcal{P}(\delta_R), \tag{13}$$

where δ_c denotes the critical threshold for collapse; then the number of collapsed objects is

$$n(M,z)dM = 2\frac{3H_0^2\Omega_m}{8\pi GM}\left|\frac{d\mathcal{P}(>\delta_c \mid z,R)}{dM}\right|M. \tag{14}$$

Note that the redshift dependence is usually enclosed only in δ_c: σ_M is computed on the field linearly extrapolated at $z = 0$, and $\delta_c(z) = \Delta_c(z)D(z = 0)/D(z)$ and $\Delta_c(z)$ depends very weakly on redshift and $\Delta_c(z = 0) \sim 1.68$.

Equation (14) however cannot be computed analytically and exactly starting from (10): some approximations need to be done in order to obtain an analytically manageable expression. Two approaches have been taken so far in the literature which we will briefly review below.

3.1. MVJ Approach. The authors of [31] proceed by first performing the integration over δ_R to obtain an exact expression for $\mathcal{P}(>\delta_c \mid z, M)$. At this point they expand the generating functional to the desired order, for example, keeping only terms up to the skewness, then perform a Wick rotation to change variables and finally a saddle-point approximation to evaluate the remaining integral. The saddle point approximation is very good for large thresholds $\delta_c/\sigma_M \gg 1$, thus for rare and massive peaks. For the final expression for the mass function they obtain

$$\begin{aligned}\hat{n}(M,z) &= 2\frac{3H_0^2\Omega_{m,0}}{8\pi GM^2}\frac{1}{\sqrt{2\pi}\sigma_M}\exp\left[-\frac{\delta_*^2}{2\sigma_M^2}\right] \\ &\quad\times\left|\frac{1}{6}\frac{\delta_c^2}{\sqrt{1-S_{3,M}\delta_c/3}}\frac{dS_{3,M}}{d\ln M}+\frac{\delta_*}{\sigma_M}\frac{d\sigma_M}{d\ln M}\right|,\end{aligned} \tag{15}$$

where σ_M denotes the *rms* value of the density field, the subscript M denotes that the density field has been smoothed

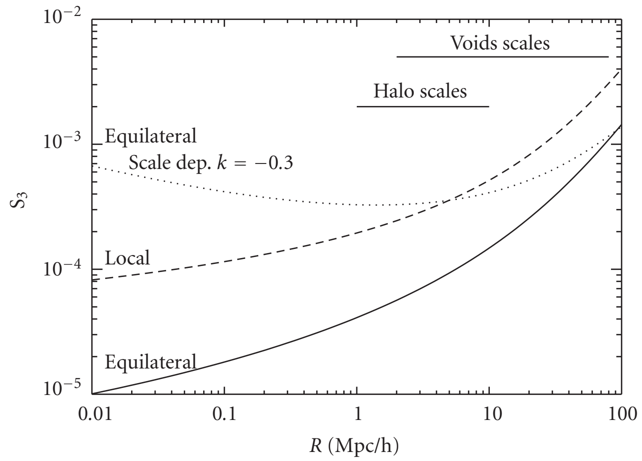

FIGURE 1: Skewness $S_{3,R}$ of the density field at $z = 0$ as a function of the smoothing scale R for different types of non-Gaussianity. Figure reproduced from [32].

on a scale $R(M)$ corresponding to $R(M) = [M3/(4\rho)]^{1/3}$, and $\delta_* = \delta_c\sqrt{1 - \delta_c S_{3,M}/3}$.

This derivation shows that the mass function in principle depends on all cumulants, but that if non-Gaussianity is described by a bispectrum (and all higher order connected correlations are assumed to be zero or at least negligible), it depends only on the skewness. The mass function does not carry explicit information about the shape of non-Gaussianity. Nevertheless for a given numerical value of $f_{\rm NL}$ the skewness can have different amplitude and scale dependence for different models of non-Gaussianity, as illustrated in Figure 1.

3.2. LMSV Approach. The authors of [9] (LMSV) instead proceed by using the saddle point approximation in the expression for $\mathcal{P}(\delta_R)$ and then using the Edgeworth expansion truncated at the desired order. The resulting simplified expression for the PDF can then be integrated to obtain $\mathcal{P}(> \delta_c \mid z, R)$ and derived to obtain the mass function. The final mass function in this approximation is given by

$$\begin{aligned}\hat{n}(M,z) = {}& 2\frac{3H_0^2\Omega_{m,0}}{8\pi GM}\frac{1}{\sqrt{2\pi}xs}\exp\left[-\frac{\delta_c^2}{2\sigma_M^2}\right] \\ & \times\left|\frac{d\ln\sigma_M}{dM}\left(\frac{\delta_c}{\sigma_M} + \frac{S_{3,M}\sigma_M}{6}\left(\frac{\delta_c^4}{\sigma_M^4} - 2\frac{\delta_c^2}{\sigma_M^2} - 1\right)\right)\right. \\ & \left. + \frac{1}{6}\frac{dS_{3,M}}{dM}\sigma_M\left(\frac{\delta_c^2}{\sigma_M^2} - 1\right)\right|. \end{aligned} \tag{16}$$

Without knowledge of all higher cumulants one is forced to use approximate expressions for the mass function. By truncating the Edgeworth expansion at the linear order in the skewness, the resulting PDF is no longer positive-definite. The number of terms that should be kept in the expansion depends on $\delta_c(z)/\sigma_M$. The truncation used is a good approximation of the true PDF if $\delta_c(z)/\sigma_M$ is small (and non-Gaussianity is small) but for rare events (the tails of the distribution) $\delta_c(z)/\sigma_M$ is large. One thus expect this approximation to break down for large masses, high redshift, and high $f_{\rm NL}$.

Reference [9] quantified the range of validity of their approximation by assuming that when terms proportional to S_3^2 become important is no longer valid to neglect terms proportional to higher-order cumulants. Then they define the validity regime of their mass function to be where corrections from the S_3^2 are unimportant. They find, as expected, that for very massive objects the approximation breaks down and that the upper mass limit for applicability of the mass function decreases with redshift and $f_{\rm NL}$. But for low masses, redshifts and $f_{\rm NL}$ their formula is better than the MVJ. On the other hand the MVJ range of validity extends to higher masses, redshifts and $f_{\rm NL}$ values, as expected, as MVJ applied the saddle point approximation to $\mathcal{P}(> \delta_c \mid M, z)$ which is an increasingly good approximation for rare objects.

Of course, the natural observable to apply this method to are not only galaxy surveys (and the clusters found there), but, especially suited, are the mass-selected large clusters surveys offered by on-going Sunyaev-Zeldovich experiments (e.g., Planck, ACT, SPT).

A detailed comparison with N-body simulations is the next logical step to pursue.

3.3. Comparison with N-Body Simulations. Before we proceed we should consider that the Press and Schechter formulation of the mass function even in the Gaussian initial conditions case, can be significantly improved see for example, [34–36]. Much improved expressions have been extensively calibrated on Gaussian initial conditions N-body simulations. The major limitations in both the MVJ and LMSV derivations (since they follow the classic Press and Schechter formulation) are the assumption of spherical collapse and the sharp k-space filtering. In addition, the excursion set improvement on the original Press and Schechter swindle relies on the random-phase hypothesis, which is not satisfied for non-Gaussian initial conditions. Since these improvements of the mass function have not yet been generalized to generic non-Gaussian initial conditions (but work is on-going, see other contributions in this issue) the analytical results above should be used to model fractional *corrections* to the Gaussian case.

Thus the non-Gaussian mass function, $n_{NG}(M,z)$ can be written as a function of a Gaussian one, $n_G(M,z)$ (accurately calibrated on N-body simulations) with a non-Gaussian *correction* factor $\mathcal{R}$ (see e.g., [9, 37]):

$$n_{NG}(M,z) = n_G(M,z)\mathcal{R}(S_3, M, z), \tag{17}$$

where

$$\mathcal{R}(S_3, M, z) = \frac{\hat{n}(M, z, f_{\rm NL})}{\hat{n}(M, z, f_{\rm NL} = 0)} \tag{18}$$

and $\hat{n}$ is given by the MVJ or LMSV approximation. The correction $\mathcal{R}$ can then be calibrated on N-body simulations.

Reference [33] argues that the same correction that is in the Gaussian case modifies the collapse threshold, δ_c, to

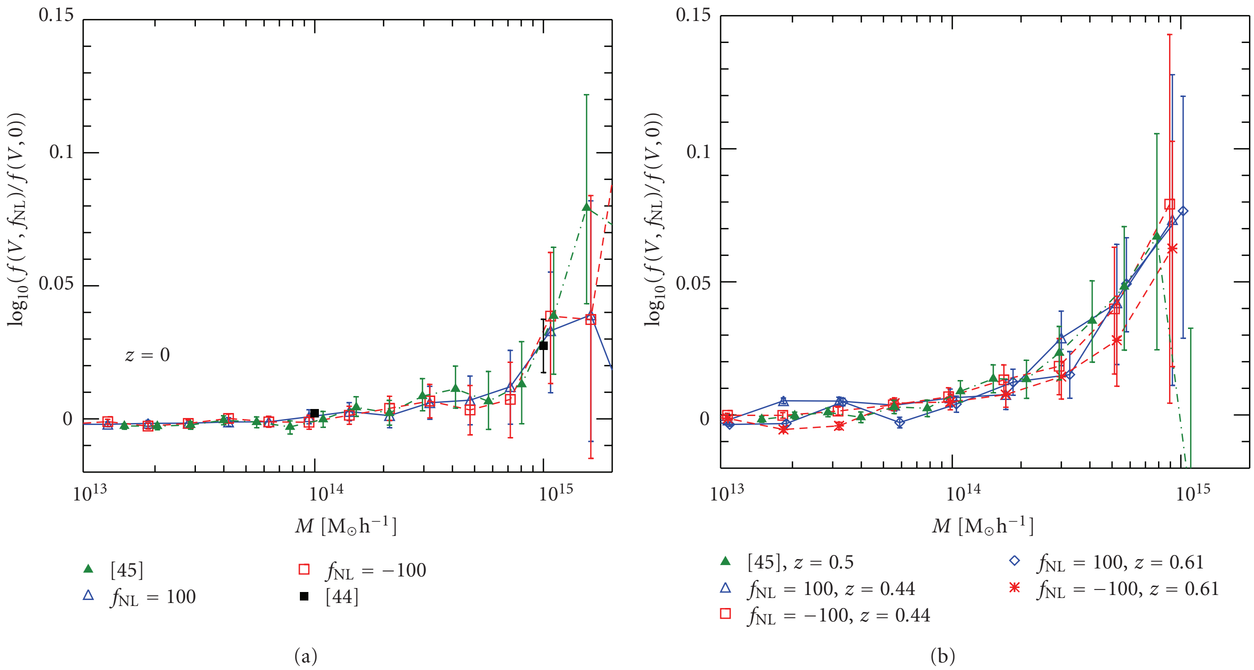

Figure 2: Correction to the Gaussian mass function as measured in different non-Gaussian simulations. There is now agreement between different simulations. The y axis should be interpreted as $\text{Log}_{10}\mathcal{R}(M, z, f_{\rm NL})$. For negative values of $f_{\rm NL}$ the absolute value of the non-Gaussian correction is considered. Reproduced from [33, Figures 4 and 5].

improve over the original Press and Schechter formulation, may apply to the non-Gaussian correction. The detailed physical interpretation of this is still matter of debate in the literature [38–40]. In summary, reference [33] proposes to write the non-Gaussian correction factor for the MVJ [31] case as

$$\mathcal{R}_{NG}(M, z, f_{\rm NL}) = \exp\left[\delta_{ec}^3 \frac{S_{3,M}}{6\sigma_M^2}\right] \times \left| \frac{1}{6} \frac{\delta_{ec}}{\sqrt{1 - \dfrac{\delta_{ec} S_{3,M}}{3}}} \frac{dS_{3,M}}{d\ln\sigma_M} + \sqrt{1 - \frac{\delta_{ec} S_{3,M}}{3}} \right|, \tag{19}$$

and for the LMSV [9] case:

$$\mathcal{R}_{NG}(M, z, f_{\rm NL}) = 1 + \frac{1}{6}\frac{\sigma_M^2}{\delta_{ec}} \times \left[S_{3,M}\left(\frac{\delta_{ec}^4}{\sigma_M^4} - 2\frac{\delta_{ec}^2}{\sigma_M^2} - 1\right) + \frac{dS_{3,M}}{d\ln\sigma_M}\left(\frac{\delta_{ec}^2}{\sigma_M^2} - 1\right)\right], \tag{20}$$

where δ_{ec} denotes the modified critical density for collapse, which for high peaks is $\delta_{ec} \sim \delta_c\sqrt{q}$. Reference [33] calibrated these expressions on N-body simulations to find $q = 0.75$. We anticipate here that the validity of this extrapolation (i.e., in terms of a correction to the critical collapse threshold) can be tested independently on the large-scale non-Gaussian halo bias as described in Section 4. Note that, in both cases, in the limit of small non-Gaussianty the correction factors reduce to

$$\mathcal{R} = 1 + S_{3,M}\frac{\delta_{ec}^3}{6\sigma_M^2}. \tag{21}$$

Non-Gaussian mass functions have been computed from simulations and compared with different theoretical predictions in several works [41–45]. In the past, conflicting results were reported, but the issue seems to have been settled, there is agreement among mass function measured from different non-Gaussian simulations performed by three different groups as shown for example in Figure 2. As expected both MVJ and LMSV prescriptions for the non-Gaussian correction to the mass function agree with the simulation results, provided one makes the substitution $\delta_c \to \delta_{ec}$, with some tentative indication that MVJ may be better for very massive objects while LMSV performs better for less rare events. This is shown in Figure 3 where the points represent measurements from N-body simulations presented in [33].

3.4. Voids. While galaxy clusters form at the highest overdensities of the primordial density field and probe the high-density tail of the PDF, voids form in the low-density regions and thus probe the low-density tail of the PDF. Most of the volume of the evolved universe is underdense, so it seems interesting to pay attention to the distribution of underdense regions. A void distribution function can be derived in an

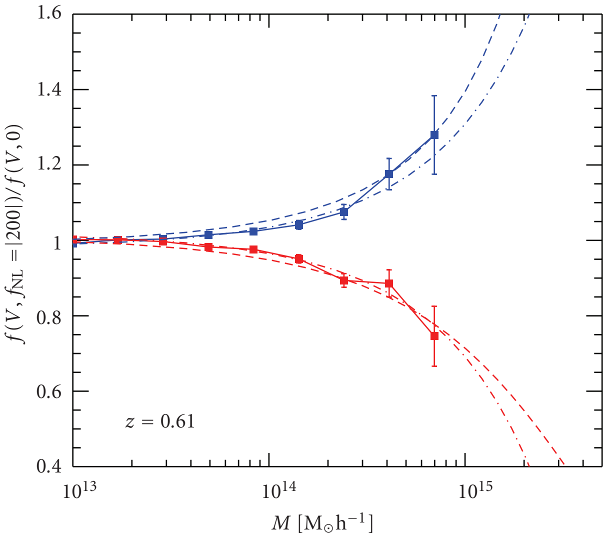

Figure 3: The points show the non-Gaussian correction to the mass function as measured in the N-body simulations of [33]. Blue corresponds to $f_{\mathrm{NL}} = 200$ and red to $f_{\mathrm{NL}} = -200$. the dashed lines correspond to the MVJ formulation and the dot-dashed lined to the LMSV formulation. In both cases the substitution $\delta_c \to \delta_{ec}$ has been performed. The y axis should be interpreted as $\mathcal{R}(M, z, f_{\mathrm{NL}} = 200)$. Reproduced from Figure 7 [33].

analogous way to the Press Schechter mass function by realizing that negative density fluctuations grow into voids [32], a critical underdensity δ_v is necessary for producing a void and this plays the role of the critical overdensity δ_c for producing bound objects (halos). The more underdense a void is the more negative δ_v becomes. The precise value of $\delta_v(z)$ depends on the precise definition of a void (and may depend on the the observables used to find voids); realistic values of $\delta_v(z = 0)$ are expected to be $\gtrsim -1$. In the absence of a better prescription, here, following [32], δ_v is treated as a phenomenological parameter and results are shown for a range of δ_v values. To derive the non-Gaussian void probability function one proceeds as above with the only subtlety that δ_v is negative and that $\mathcal{P}(< \delta) = 1 - \mathcal{P}(> \delta)$ thus $|d\mathcal{P}(< \delta)/dM| = |d\mathcal{P}(> \delta)/dM|$. Thus the void PDF as a function of $|\delta_v|$ can be obtained from the PDF of MVJ [31] or LMSV [9], provided one keeps track of the sign of each term. For example in the LMSV approximation the void distribution function becomes [32]

$$\begin{aligned}\hat{n}(R, z, f_{\mathrm{NL}}) = {} & \frac{9}{2\pi^2}\sqrt{\frac{\pi}{2}}\frac{1}{R^4}e^{-\delta_v^2/2\sigma_M^2} \\ & \times \left\{ \left| \frac{d\ln\sigma_M}{d\ln M} \right| \right. \\ & \quad \times \left[-\frac{|\delta_v|}{\sigma_M}\frac{S_{3,M}\sigma_M}{6}\left(\frac{\delta_v^4}{\sigma_M^4} - 2\frac{\delta_v^2}{\sigma_M^2} - 1\right)\right] \\ & \quad \left. + \frac{1}{6}\frac{dS_3}{dM}\sigma_M\left(\frac{\delta_v^2}{\sigma_M^2} - 1\right)\right\},\end{aligned} \tag{22}$$

where the expression is reported as a function of the smoothing radius rather than the mass, since a void Lagrangian radius is probably easier to determine than its mass.

Note that while a positive skewness ($f_{\mathrm{NL}} > 0$) boosts the number of halos at the high-mass end (and slightly suppress the number of low-mass halos), it is a negative skewness that will increase the voids size distribution at the largest voids end (and slightly decrease it for small void sizes). Reference [32] concluded that the abundance of voids is sensitive to non-Gaussianity, $|\delta_v|$ is expected to be smaller than δ_c by a factor 2 to 3. If voids probe the same scales as halos then they should provide constraints on f_{NL}2 to 3 times worse. However voids may probe slightly larger scales than halos, in many non-Gaussian models, $S_3^{f_{\mathrm{NL}}=1}$ increases with scales (see e.g., Figure 1), compensating for the threshold.

The approach reviewed here provides a rough estimate of the fractional change in abundance due to primordial non-Gaussianity but will not provide reliably the abundance itself. It is important to stress here that rigorously quantitative results will need to be calibrated on cosmological simulations and mock survey catalogs.

4. Effects on the Halo Power Spectrum

Recently, reference [43, 46] showed that primordial non-Gaussianity affects the clustering of dark matter halos (i.e., density extrema) inducing a scale-dependent bias for halos on large scales. This can be seen for example by considering halos as regions where the (smoothed) linear density field exceeds a suitable threshold. All correlations and peaks considered in the section are those of the *initial* density field (linearly extrapolated to the present time). Thus for example in the Gaussian case [47–49] for high peaks we would have the following relation between the correlation function of halos of mass M, $\xi_{h,M}(r)$ and that of the dark matter distribution smoothed on scale R, corresponding to mass M, $\xi_R(r)$:

$$\xi_{h,M}(r) \simeq \left(b_{h,L}^G\right)^2 \xi_R(r), \tag{23}$$

where $b_L^G \simeq \delta_c/\sigma_R^2$ denotes the Lagrangian halo bias (in the Gaussian case), although more refined expressions can be found in for example, [50, 51].

The Lagrangian bias appears here because correlations and peaks are those of the initial density field (lineary extrapolated). Making the standard assumptions that halos move coherently with the underlying dark matter, one can obtain the final Eulerian bias as $b_E = 1 + b_L$, using the techniques outlined in [50–53]. Below we will omit the subscript E for Eulerian bias.

The two-point correlation function of regions above a high threshold has been obtained, for the general non-Gaussian case, in [54–56]:

$$\xi_{h,M}(|\mathbf{x}_1 - \mathbf{x}_2|) = -1 + \exp[X], \tag{24}$$

where

$$X = \sum_{N=2}^{\infty}\sum_{j=1}^{N-1}\frac{\nu^N\sigma_R^{-N}}{j!(N-j)!}\xi^{(N)}\Bigg[\underbrace{\mathbf{x}_1,\ldots,\mathbf{x}_1}_{j\ \text{times}}, \underbrace{\mathbf{x}_2,\ldots,\mathbf{x}_2}_{(N-j)\ \text{times}}\Bigg], \tag{25}$$

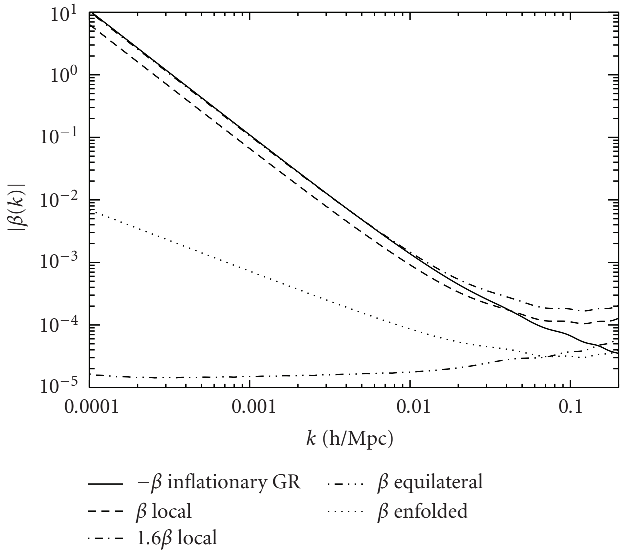

FIGURE 4: The scale-dependence of the large-scale halo bias induced by a nonzero bispectrum for different types of non-Gaussianity. The dashed line corresponds to the local type and the dot-dot-dot-dashed to equilateral type. Figure reproduced from [57].

where $\nu = \delta_c \sigma_R$. For large separations the exponential can be expanded to first order. This is what we will do in what follows but we will comment on this choice below.

For small non-Gaussianities (Effectively that is for values of $f_{\rm NL}$ consistent with observations.), we can keep terms up to the three-point correlation function $\xi^{(3)}$, obtaining that the correction to the halo correlation function, $\Delta\xi_h$ due to a non-zero three-point function is given by:

$$\begin{aligned}\Delta\xi_h &= \frac{\nu_R^3}{2\sigma_R^3}\left[\xi_R^{(3)}(\mathbf{x}_1,\mathbf{x}_2,\mathbf{x}_2)+\xi_R^{(3)}(\mathbf{x}_1,\mathbf{x}_1,\mathbf{x}_2)\right]\\ &= \frac{\nu_R^3}{\sigma_R^3}\xi_R^{(3)}(\mathbf{x}_1,\mathbf{x}_1,\mathbf{x}_2).\end{aligned} \tag{26}$$

For a general bispectrum $B(k_1, k_2, k_3)$ this yields a correction to the power spectrum (see [46] for steps in the derivation):

$$\begin{aligned}\frac{\Delta P}{P} &= \frac{\delta_c(z)}{\mathcal{M}_R(k)}\frac{1}{4\pi^2\sigma_R^2}\int dk_1 k_1^2 \mathcal{M}_R(k_1)\\ &\quad\times\int_{-1}^{1} d\mu \mathcal{M}_R(\sqrt{\alpha})\frac{\beta_\phi(k_1,\sqrt{\alpha},k)}{P_\phi(k)},\end{aligned} \tag{27}$$

where we have made the substitution $\alpha = k_1^2+k^2+2k_1k\mu$. Here $\mathcal{M}_R = W_R\mathcal{M}$ and W_R and $\mathcal{M}$ were introduced in Section 3. The effect on the halo bias is $\Delta b_h^L/b_h^L = (1/2)(\Delta P/P)$ and thus

$$b_h^{f_{\rm NL}} = 1 + \frac{\Delta_c(z)}{\sigma_R^2 D^2(z)}\left[1+\delta_c(z)\beta_R(k)\right], \tag{28}$$

where the expression for β can be obtained by comparing to (27). The term $\Delta_c(z)/[\sigma_R^2 D^2(z)] \simeq b^G - 1$ can be recognized as the Gaussian Lagrangian halo bias.

So far the derivation is generic for all types of non-Gaussianity specified by a given bispectrum. We can then consider specific cases. In particular for local non-Gaussianity we obtain

$$\begin{aligned}\beta_R(k) &= \frac{2f_{\rm NL}}{8\pi^2\sigma_R^2\mathcal{M}_R(k)}\int dk_1 k_1^2\mathcal{M}_R(k_1)P_\phi(k_1)\\ &\quad\times\int_{-1}^{1} d\mu\mathcal{M}_R(\sqrt{\alpha})\left[\frac{P_\phi(\sqrt{\alpha})}{P_\phi(k)}+2\right].\end{aligned} \tag{29}$$

Thus $\Delta b_h/b_h$ is $2f_{\rm NL}$ times a redshift-dependent factor $\Delta_c(z)/D(z) = \delta_c(z)$, times a k- and mass-dependent factor. The function $\beta_R(k)$ is shown as the dashed line in Figure 4. This result for the local non-Gaussianity has been derived in at least three other ways. Reference [43] generalizes the Kaiser [47] argument of high peak bias for the local non-Gaussianity. Starting from $\nabla^2\Phi = \nabla^2\phi + 2f_{\rm NL}[\phi\nabla^2\phi + |\nabla\phi|^2]$ where near peaks $|\nabla\phi|^2$ is negligible they obtain $\delta = \delta^{f_{\rm NL}=0}[1+2f_{\rm NL}\phi]$. The Poisson equation to convert ϕ in δ then gives the scale-dependence. More details are presented elsewhere in this issue.

Reference [58] works in the peak-background split. This approach is especially useful to understand that it is the coupling between very large and small scales introduced by local (squeezed-configurations) non-Gaussianity to boost (or suppress) the peaks clustering. In this approach, the density field can be written as $\rho(\vec{x}) = \overline{\rho}(1+\delta_l+\delta_s)$ where δ_l denotes long wavelength fluctuations and δ_s short wavelength fluctuations. δ_l is the one responsible for modulating halo formation (i.e., to boost peaks above the threshold for collapse), so the halo number density is $n = \overline{n}(1+b_{h,L}\delta_l)$ and $b_{h,L} = \overline{n}^{-1}\partial n/\partial\delta_l$.

In the local non-Gaussian case they decompose the Gaussian field ϕ as a combination of long and short wavelength fluctuations $\phi = \phi_l + \phi_s$ thus $\Phi = \phi_l + f_{\rm NL}\phi_l^2 + (1+2f_{\rm NL}\phi_l)\phi_s + f_{\rm NL}\phi_s^2 + const$. Also in this non-Gaussian case one can split the density field δ in δ_l and δ_s and relate this to $f_{\rm NL}$ (it is easier to work in Fourier space): $\delta_l(k) = \alpha(k)\phi_l(k)$ and $\delta_s = \alpha(k)[(1+2f_{\rm NL}\phi_l)\phi_s + f_{\rm NL}\phi^2] \equiv \alpha(k)[X_1\phi_s + X_2\phi_s^2]$, the last equality giving the definition of X_1 and X_2. Note that δ_s cannot be ignored here because ϕ_l enters in X_1, in other words, local non-Gaussianity couples long and short wavelength modes. The local halo number density is now function of δ_l, X_1, and X_2 yielding the following result for the Lagrangian halo bias:

$$\begin{aligned}b_{h,L} &= \overline{n}^{-1}\left[\frac{\partial n}{\partial\delta_l}+2f_{\rm NL}\frac{{\rm d}\phi_l}{{\rm d}\delta_l}\frac{\partial n}{\partial X_1}\right]\\ &= b_{h,L}^G + 2f_{\rm NL}\frac{{\rm d}\phi_l}{{\rm d}\delta_l}\frac{\partial\ln n}{\partial\ln\sigma_8}\\ &\equiv b_{h,L}^G\left(1+2f_{\rm NL}\alpha(k)^{-1}\delta_c\right),\end{aligned} \tag{30}$$

where $\alpha(k)$ encloses the scale-dependence of the effect. Reference [59] rederives the ellipsoidal collapse for small deviations from Gaussianity of the local type. They find that a non-zero $f_{\rm NL}$ modifies the threshold for collapse, the modification is proportional to $f_{\rm NL}$. This should sound familiar from Section 3. They then use the definition $b_{h,L} = \overline{n}^{-1}\partial n/\partial\delta_c$ keeping track of the fact that δ is "modulated" by $f_{\rm NL}$.

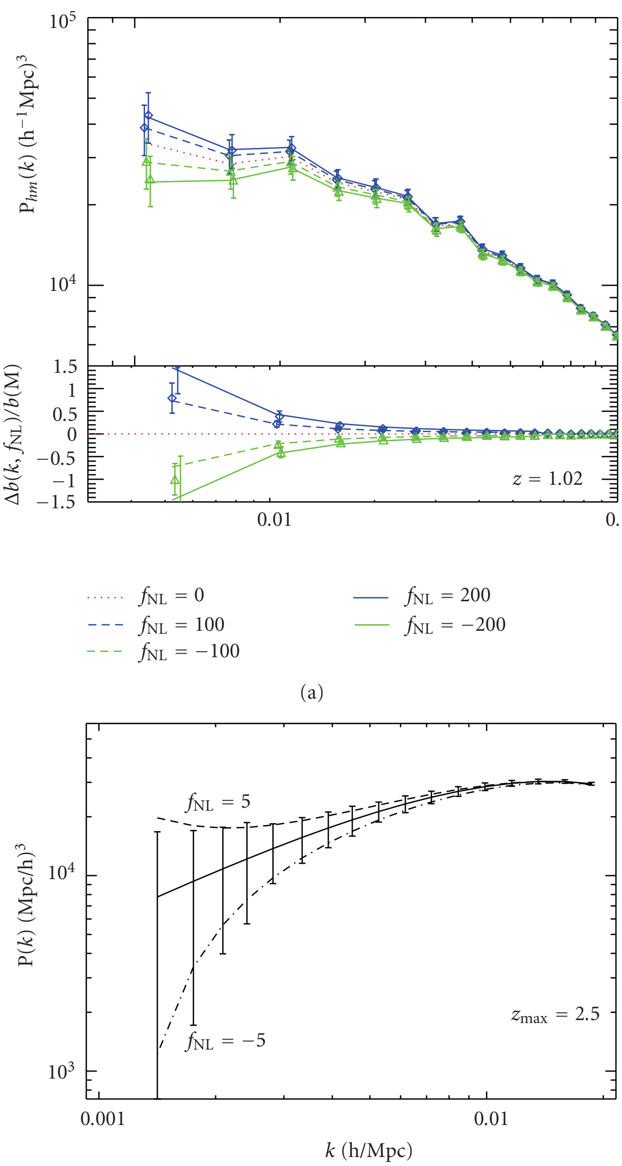

(a)

(b)

FIGURE 5: Effect of the non-Gaussian halo bias on the power spectrum. In the left-top of (a) panel we show the halo-matter cross-power spectrum for masses above $10^{13}\,M_\odot$ at $z = 1.02$. The left-bottom panel of (a) shows the ratio of the non-Gaussian to Gaussian bias. Figure reproduced from [33]. The f_{NL} values reported in the figure legend should be interpreted as f_{NL}^{LSS}. On the right panel we show the expected effect and error-bars for the large-scale power spectrum for a survey like LSST. Figure reproduced from [26].

The effect of the non-Gaussian halo bias on the power spectrum is shown in Figure 5 where the points are measurements from an N-body simulations of [33] (see figure caption for more details).

The above result

$$\Delta b = f_{NL}\delta_c\left(b_h^G - 1\right)\beta_R^{f_{NL}=1}(k), \tag{31}$$

where $\beta_R(k) = f_{NL}\beta_R^{f_{NL}=1}(k)$, can be improved in several ways.

First of all, we have not made any distinction between the redshift at which the object is being observed (z_o) and that at which is being formed (z_f). Except for the rarest events this should be accounted for. The Gaussian Lagrangian bias expression used so far is an approximation, a more accurate expression is [50, 52, 53]

$$b_{h,L}^G\left(z_o, M, z_f\right) = \frac{1}{D(z_o)}\left[\frac{\delta_c\left(z_f\right)}{\sigma_M^2} - \frac{1}{\delta_c\left(z_f\right)}\right]. \tag{32}$$

Then, the halo bias expressions are derived within the "classical" Press and Schechter theory, as we have seen in Section 3, subsequent improvements on the mass function can be seen as a correction to the collapse threshold. In the expression for the Gaussian halo bias $b_L^G = \overline{n}^{-1}\partial n^G/\partial\delta_c$ one can consider mass functions that are better fit to simulations than the standard Press and Schecter one obtaining:

$$b_{h,L}^G\left(z_o, M, z_f\right) = \frac{1}{D(z_o)}\left[\frac{q\delta_c\left(z_f\right)}{\sigma_M^2} - \frac{1}{\delta_c\left(z_f\right)}\right] + \frac{2p}{\delta_c\left(z_f\right)D(z_0)}\left[1 + \left(\frac{q\delta_c^2\left(z_f\right)}{\sigma_M^2}\right)^p\right]^{-1}. \tag{33}$$

The parameters q and p account for nonspherical collapse and fit to numerical simulations yield $q \sim 0.75$, $p = 0.3$ for example, [34]. In this expression the term in the second line is usually subdominant. The term "$-1/\delta_c$" in the first line is known as "antibias", and it becomes negligible for old halos $z_f \gg z_o$. Note that by including the antibias correction in b_g of (31) one recovers the "recent mergers" approximation of [58].

The same correction should also apply to the non-Gaussian correction to the halo bias:

$$\Delta b = f_{NL}q'\delta_c\left(b_h^G - 1\right)\beta_R^{f_{NL}=1}(k), \tag{34}$$

where q' should coincide with q above; it can be calibrated to N-body simulations and is found indeed to be $q' = 0.75$ [33]. The non-Gaussian halo bias prediction and results from N-body simulations with local non-Gaussianity are shown in Figure 6.

Finally one may note that for f_{NL} large and negative, (27) and (28) would formally yield $b_h^{f_{NL}}$ and $P_h(k)$ negative on large enough scales. This is a manifestation of the breakdown of the approximations made: (a) all correlations of higher order than the bispectrum were neglected, for large NG this truncation may not hold; (b) The exponential in (24) was expanded to linear order. This however could be easily corrected for, remembering that the $P(k)$ obtained from (27) is in reality the Fourier transform of X, the argument of the exponential. One would then compute the halo correlation function using (24) and Fourier transforming back to obtain the halo power-spectrum.

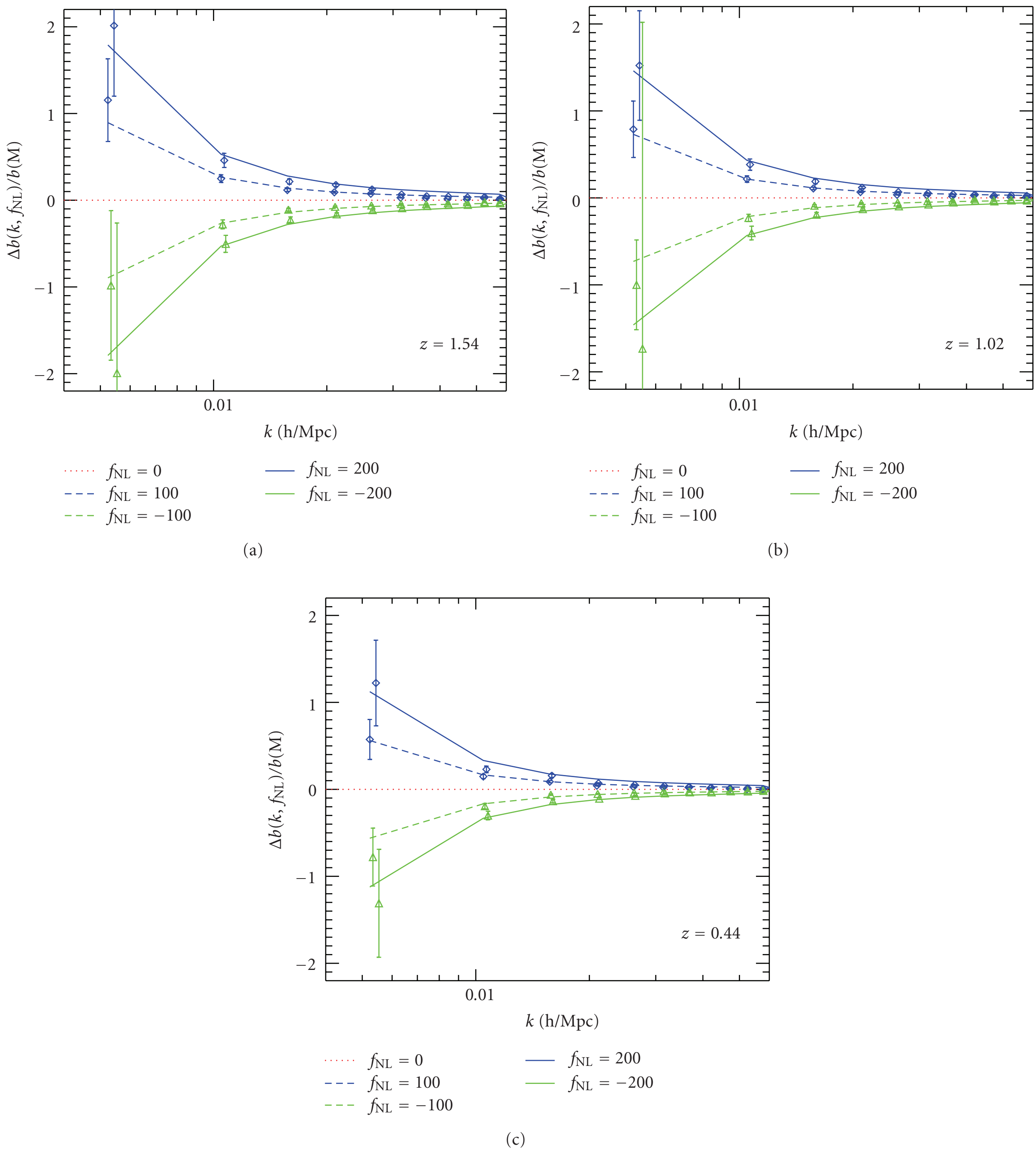

FIGURE 6: The quantity $\Delta b/b$ as function of k, for simulation snapshots at $z = 0.44$, 1.02, and 1.54. Simulation outputs and theory lines are shown for $f_{NL} = \pm 100$ and $f_{NL} = \pm 200$. Figure reproduced from [33]. The f_{NL} values reported in this figure legend should be interpreted as f_{NL}^{LSS}.

So far we have concentrated on local non-Gaussianity, but the expression of (27) and (28) is more general. Using this formulation, reference [57] computed the quantity $\beta_R^{f_{NL}=1}(k)$ for several types of non-Gaussianity (equilateral, local, and enfolded); this is shown in Figure 4. It is clear that the non-Gaussian halo-bias effect has some sensitivity to the bispectrum shape, for example the effect for the equilateral type of non-Gaussianity is suppressed by orders of magnitude compared to the local-type and the flattened case is somewhere in the middle. Figure 4 also shows a type of non-Gaussianity arising from General-relativistic (GR) corrections on scales comparable to the Hubble radius. Note that perturbations on super-Hubble scales are initially needed in order to "feed" the GR correction terms. In this respect the significance of this contribution is analogous to the well-known large-scale anticorrelation between CMB

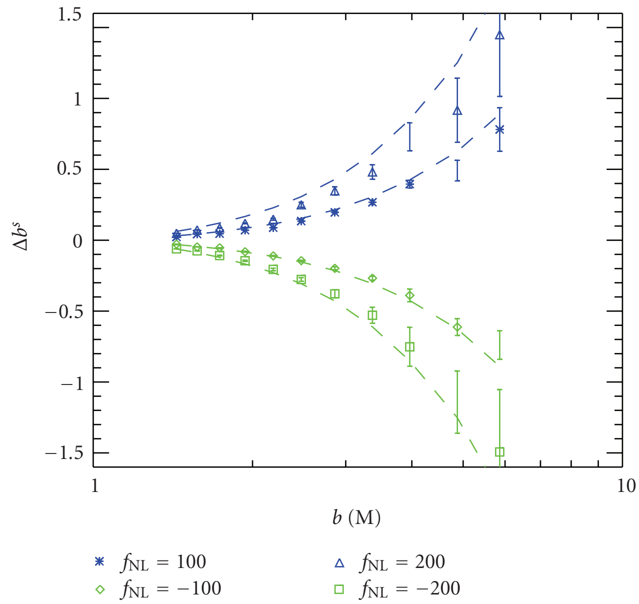

Figure 7: Non-Gaussian halo bias correction as function of the gaussian halo bias. Figure reproduced from [33]. The f_{NL} values reported in the figure legend should be interpreted as $f_{\mathrm{NL}}^{\mathrm{LSS}}$.

Table 1: Current recent $2-\sigma$ constraints on local f_{NL}.

Data/method	f_{NL}	Reference
Photometric LRG-bias	63^{+101}_{-331}	[58]
Spectroscopic LRG-bias	70^{+139}_{-191}	[58]
QSO-bias	8^{+47}_{-77}	[58]
Combined	28^{+42}_{-57}	[58]
NVSS-ISW	105^{+755}_{-1157}	[58]
NVSS-ISW	$236 \pm 127(1-\sigma)$	[59]
WMAP3-Bispectrum	30 ± 84	[10]
WMAP3-Bispectrum	32 ± 68	[8]
WMAP3-Bispectrum	87 ± 60	[20]
WMAP-Bispectrum	38 ± 42	[11, 17, 21]
WMAP5-Bispectrum	51 ± 60	[10]
WMAP5-Minkowski	-57 ± 121	[10]

Table 2: Forecasts $1-\sigma$ constraints on local f_{NL}.

Data/method	Δf_{NL} $(1-\sigma)$	Reference
BOSS-bias	18	[63]
ADEPT/Euclid-bias	1.5	[63]
PANNStarrs-bias	3.5	[63]
LSST-bias	0.7	[63]
LSST-ISW	7	[59]
BOSS-bispectrum	35	[27]
ADEPT/Euclid-bispectrum	3.6	[27]
Planck-Bispectrum	3	[19]
BPOL-Bispectrum	2	[19]

temperature and E-mode polarization, it is a consequence of the properties of the inflationary mechanism to lay down the primordial perturbations. This effect has the same magnitude as a local non-Gaussianity with $f_{\mathrm{NL}} \gtrsim 1$.

The next logical step is then to ask how well present or forthcoming data could constrain non-Gaussianity using the halo-bias effect. It is interesting to note that surveys that aim at measuring Baryon Acoustic Oscillations (BAO) in the galaxy distribution to constrain dark energy are well suited to also probe non-Gaussianity; they cover large volumes and their galaxy number density is well suited so that on the scale of interest (both for BAO and non-Gaussianity) shot noise does not dominate the signal. Photometric surveys are also well suited: as the non-Gaussian signal is localized at very large scales and is a smooth function of k, the photo-z smearing effects are unimportant.

The theory developed so far describes the clustering of halos while we observe galaxies. Different galaxy populations occupy dark matter halos following different prescriptions. If we think in the halo-model framework (e.g., [60] and references therein) at very large scales only the “two-halo” contribution matters and the details of the halo occupation distribution (the “one-halo” term) become unimportant.

What is important to keep in mind is that the effect of the non-Gaussianity parameter one wants to measure, f_{NL}, is fully degenerate with the value of the Gaussian (small scales) halo bias. Figure 7 shows the dependence of the non-Gaussian correction on the Gaussian bias.

Thus highly biased tracers will show a larger non-Gaussian effect for the same f_{NL} value. Of course for a given cosmological model the Gaussian bias can be measured accurately by comparing the predicted dark matter power spectrum with the observed one. Alternatively, two differently biased tracers can be used in tandem to disentangle the two effects [61, 62].

Since clustering amplitude may depend on the entire halo history, it becomes then interesting to model in details the dependence of the effect on the halo merger tree (Reid et al., in preparation).

4.1. Outlook for the Future. How well can this method do to constrain primordial non-Gaussianity compared with the other techniques presented here? The Integrated Sachs Wolfe (ISW) effect offers a window to probe clustering on the largest scales (where the signal is large); on the other hand, a measurement of clustering of tracers of dark matter halos is a very direct window into this effect. A Fisher matrix approach [58, 59, 63] shows that the ISW signal is weighted at relatively low redshift (where dark energy starts dominating) while the non-Gaussian signal grows with redshift, thus making the shape of the halo power spectrum a more promising tool. An overview of current constraints from different approaches can be found in Table 1 and future forecasts in Table 2, for non-Gaussianity of the local type. Large, mass-selected cluster samples as produced by SZ-based experiments will provide a optimally suited data-set for this technique (see e.g., [64]).

While for a given f_{NL} model such as the local one, methods that exploit the non-Gaussian bias seem to yield the smallest error-bars for large-scale structure, it should be kept in mind that the bispectrum can be used to investigate the full configuration dependence of $f_{\rm NL}$ and thus is a very powerful tool to discriminate between different type of non-Gaussianity. In addition CMB-bispectrum and halo bias test non-Gaussianity on very large scales while the large scale structure bispectrum mostly probes mildly nonlinear scales. As primordial non-Gaussianity may be scale-dependent, all these techniques are highly complementary.

The above estimates assume that the underlying cosmological model is known. The large-scale shape of the power spectrum can be affected by cosmology. Carbone et al. (in prep.) explore possible degeneracies between $f_{\rm NL}$ and cosmological parameters. They find that the parameters that are most strongly correlated with $f_{\rm NL}$ are parameters describing dark energy clustering, neutrino mass and running of the primordial power spectrum spectral slope. For surveys that cover a broad redshift range the error on $f_{\rm NL}$ degrade little when marginalizing over these extra parameters; the peculiar redshift dependence of the non-Gaussian signal lifts the degeneracy.

5. Conclusions

A natural question to ask at this point may be "what observable will have better chances to constrain primordial non-Gaussianity?"

In principle the abundance of rare events is a very powerful probe of non-Gaussianity; however, in practice, it is limited by the practical difficulty of determining the mass of the observed objects and its corresponding large uncertainty in the determination. This point is stressed for example, in [9]. With the advent of high-precision measurements of gravitational lensing by massive clusters, the mass uncertainty, at least for small to moderate size clusters samples can be greatly reduced. Forthcoming Sunyaev-Zeldovich experiments will provide large samples of mass-selected clusters which could then be followed up by lensing mass measurements (see e.g., [65, 66]). So far there is only one very high redshift ($z = 1.4$) very massive $M \simeq 8 \times 10^{14} M_{\odot}$ with high-precision mass determination via gravitational lensing [67]. Reference [68] pointed out that this object is extremely rare, for Gaussian initial conditions there should be 0.002 such objects or less in the surveyed area, which is uncomfortably low probability. But the cluster mass is very well determined; a non-Gaussianity still compatible with CMB constraints could bring the probability of observing of the object to more comfortable values. This result should be interpreted as a "proof of principle" showing that this a potentially powerful avenue to pursue.

The measurement of the three-point correlation function allows one to map directly the shape-dependence of the bispectrum. For large-scale structures the limiting factors are the large non-Gaussian contribution induced by gravitational evolution and the uncertainly of the nonlinear behavior of galaxy bias.

The halo-bias approach can yield highly competitive constraints, but it is less sensitive to the bispectrum shape. Still, the big difference in the magnitude and shape of

Table 3: Forecasted non-Gaussianity constraints: (A) [20] (B) [63] (C) [69, 70] (E) [57]) (F) e.g., [15].

	CMB Bispectrum		Halo bias	
type NG	Planck	BPol	Euclid	LSST
		$1-\sigma$ errors		
Local	$3^{(A)}$	$2^{(A)}$	$1.5^{(B)}$	$0.7^{(B)}$
Equilateral	$25^{(C)}$	$14^{(C)}$	—	—
Enfolded	$\mathcal{O}10$	$\mathcal{O}10$	$39^{(E)}$	$18^{(E)}$
		$\#\sigma$ detection		
GR	N/A	N/A	$1^{(E)}$	$2^{(E)}$
secondaries	$3^{(F)}$	$5^{(F)}$	N/A	N/A

the scale-dependent biasing factor between different non-Gaussian models implies that the halo bias can become a useful tool to study shapes when combined with for example, measurements of the CMB bispectrum. Table 3 highlights this complementarity. For example, one could envision different scenarios.

If non-Gaussianity is local with negative $f_{\rm NL}$ and CMB obtains a detection, then the halo bias approach should also give a high-significance detection (GR correction and primordial contributions add up), while if it is local but with positive $f_{\rm NL}$, the halo-bias approach could give a lower statistical significance for small $f_{\rm NL}$ as the GR correction contribution has the opposite sign.

If CMB detects $f_{\rm NL}$ at the level of $\sim$ 10 and of a form that is close to local, but halo bias does not detect it, then the CMB bispectrum is given by secondary effects.

If CMB detects non-Gaussianity but is not of the local type, then halo bias can help discriminate between equilateral and enfolded shapes; if halo bias sees a signal it indicates enfolded type; if halo bias does not see a signal it indicates equilateral type. Thus even a nondetection of the halo-bias effect, in combination with CMB constraints can have an important discriminatory power.

In any case, if the simplest inflationary scenario holds, for surveys like Euclid and LSST, the halo-bias approach is expected to detect a non-Gaussian signal very similar to the local type signal with an amplitude of $f_{\rm NL} \sim -1.5$ which is due to large-scales GR corrections to the Poisson equation. This effect should leave no imprint in the CMB; once again the combination of the two observable can help enormously to discriminate among models for the origin of cosmological structures.

In addition we should bear in mind that non-Gaussianity may be scale-dependent. In fact for models like DBI inflation it is expected to be scale-dependent. A proposed parameterization of the scale-dependence of non-Gaussianity is given by

$$B_{\phi}\left(\vec{k}_1, \vec{k}_2, \vec{k}_3\right) = f_{\rm NL}\left(\frac{K}{k_p}\right)^{n_{ng}} F\left(\vec{k}_1, \vec{k}_2, \vec{k}_3\right), \tag{35}$$

where $K = (k_1 k_2 k_3)^{1/3}$ [70], k_p denotes the pivot and n_{ng} the slope or running of non-Gaussianity, although other authors prefer to use $K = (k_1 + k_2 + k_3)/3$ [9, 59] as for

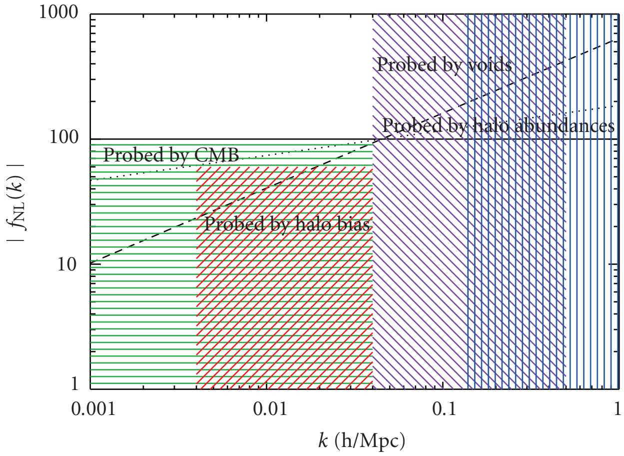

Figure 8: Scale-dependent f_{NL} and scales probed by different approaches mentioned here. The solid line has $n_g = 0$, the dotted line has $n_g = 0.2$, and the dashed one has $n_g = 0.6$. Hashed areas for CMB and halo-bias show allowed regions.

squeezed configurations $K \neq 0$. It is still an open issue which parameterization is better in practice.

In any case different observables probe different scales (see Figure 8) and their complementary means that "the combination is more than the sum of the parts."

What is clear, however, is that the thorny systematic effects that enter in all these approaches will require that a variety of complementary avenues be taken to establish a robust detection of primordial non-Gaussianity.

Acknowledgments

This work is supported by MICCIN Grant AYA2008-03531 and FP7-IDEAS-Phys.LSS 240117. The author would like to thank her closest collaborators in many of the articles reviewed here: Carmelita Carbone, Klaus Dolag, Margherita Grossi, Alan Heavens, Raul Jimenez, Marc Kamionkowski, Marilena LoVerde, Sabino Matarrese, Lauro Moscardini, Sarah Shandera, and her collaborators for the reported work-in-progress: Carmelita Carbone, Olga Mena, Beth Reid. She would also like to thank the referee for a careful review of the manuscript.

References

[1] N. Bartolo, E. Komatsu, S. Matarrese, and A. Riotto, "Non-Gaussianity from inflation: theory and observations," *Physics Reports*, vol. 402, no. 3-4, pp. 103–266, 2004.

[2] D. S. Salopek and J. R. Bond, "Nonlinear evolution of long-wavelength metric fluctuations in inflationary models," *Physical Review D*, vol. 42, no. 12, pp. 3936–3962, 1990.

[3] A. Gangui, F. Lucchin, S. Matarrese, and S. Mollerach, "The three-point correlation function of the cosmic microwave background in inflationary models," *The Astrophysical Journal*, vol. 430, no. 2, pp. 447–457, 1994.

[4] L. Verde, L. Wang, A. F. Heavens, and M. Kamionkowski, "Large-scale structure, the cosmic microwave background and primordial non-Gaussianity," *Monthly Notices of the Royal Astronomical Society*, vol. 313, no. 1, pp. 141–147, 2000.

[5] E. Komatsu and D. N. Spergel, "Acoustic signatures in the primary microwave background bispectrum," *Physical Review D*, vol. 63, no. 6, Article ID 063002, 2001.

[6] D. Babich, P. Creminelli, and M. Zaldarriaga, "The shape of non-Gaussianities," *Journal of Cosmology and Astroparticle Physics*, no. 8, pp. 199–217, 2004.

[7] P. Creminelli, A. Nicolis, L. Senatore, M. Tegmark, and M. Zaldarriaga, "Limits on non-Gaussianities from WMAP data," *Journal of Cosmology and Astroparticle Physics*, no. 5, article 004, 2006.

[8] P. Creminelli, L. Senatore, M. Zaldarriaga, and M. Tegmark, "Limits on fNL parameters from Wilkinson Microwave Anisotropy Probe three-year data," *Journal of Cosmology and Astroparticle Physics*, no. 3, article 005, 2007.

[9] M. LoVerde, A. Miller, S. Shandera, and L. Verde, "Effects of scale-dependent non-Gaussianity on cosmological structures," *Journal of Cosmology and Astroparticle Physics*, vol. 2008, no. 4, article 014, 2008.

[10] E. Komatsu, J. Dunkley, M. R. Nolta, et al., "Five-year Wilkinson microwave anisotropy probe (WMAP) observations: cosmological interpretation," *The Astrophysical Journal Supplement Series*, vol. 180, no. 2, article 330.

[11] E. Komatsu, N. Afshordi, N. Bartolo, et al., "Non-Gaussianity as a probe of the physics of the primordial universe and the astrophysics of the low redshift universe," in *AGB Stars and Related Phenomenastro: The Astronomy and Astrophysics Decadal Survey*, vol. 2010 of *Astronomy*, p. 158, 2009.

[12] D. M. Goldberg and D. N. Spergel, "Microwave background bispectrum. II. A probe of the low redshift universe," *Physical Review D*, vol. 59, no. 10, Article ID 103002, 6 pages, 1999.

[13] L. Verde and D. N. Spergel, "Dark energy and cosmic microwave background bispectrum," *Physical Review D*, vol. 65, no. 4, Article ID 043007, 2002.

[14] A. Cooray and W. Hu, "Weak gravitational lensing bispectrum," *The Astrophysical Journal*, vol. 548, pp. 7–18, 2001.

[15] A. Mangilli and L. Verde, "Non-Gaussianity and the CMB bispectrum: confusion between primordial and lensing-Rees-Sciama contribution?" *Physical Review D*, vol. 80, no. 12, Article ID 123007, 2009.

[16] P. Serra and A. Cooray, "Impact of secondary non-Gaussianities on the search for primordial non-Gaussianity with CMB maps," *Physical Review D*, vol. 77, no. 10, Article ID 107305, 2008.

[17] D. Hanson, K. M. Smith, A. Challinor, and M. Liguori, "CMB lensing and primordial non-Gaussianity," *Physical Review D*, vol. 80, no. 8, Article ID 083004, 2009.

[18] A. P. S. Yadav and B. D. Wandelt, "CMB tomography: reconstruction of adiabatic primordial scalar potential using temperature and polarization maps," *Physical Review D*, vol. 71, no. 12, Article ID 123004, 2005.

[19] A. P. S. Yadav, E. Komatsu, and B. D. Wandelt, "Fast estimator of primordial non-Gaussianity from temperature and polarization anisotropies in the cosmic microwave background," *The Astrophysical Journal*, vol. 664, no. 2, pp. 680–686, 2007.

[20] A. P. S. Yadav and B. D. Wandelt, "Evidence of primordial non-Gaussianity (fNL) in the wilkinson microwave anisotropy probe 3-year data at 2.8σ," *Physical Review Letters*, vol. 100, no. 18, Article ID 181301, 2008.

[21] K. M. Smith, L. Senatore, and M. Zaldarriaga, "Optimal limits on f_{NL}^{local} from WMAP 5-year data," *Journal of Cosmology and Astro-Particle Physics*, vol. 9, article 006, 2009.

[22] P. Chingangbam and C. Park, "Statistical nature of non-Gaussianity from cubic order primordial perturbations: CMB map simulations and genus statistic," *Journal of Cosmology and Astroparticle Physics*, vol. 2009, no. 12, article 019, 2009.

[23] P. Catelan, F. Lucchin, S. Matarrese, and L. Moscardini, "Eulerian perturbation theory in non-flat universes: second-order approximation," *Monthly Notices of the Royal Astronomical Society*, vol. 276, pp. 39–56, 1995.

[24] S. Matarrese, L. Verde, and A. F. Heavens, "Large-scale bias in the universe: bispectrum method," *Monthly Notices of the Royal Astronomical Society*, vol. 290, no. 4, pp. 651–662, 1997.

[25] L. Verde, A. F. Heavens, and S. Matarrese, "Projected bispectrum in spherical harmonics and its application to angular galaxy catalogues," *Monthly Notices of the Royal Astronomical Society*, vol. 318, no. 2, pp. 584–595, 2000.

[26] LSST Science Collaborations, "LSST Science Book, Version 2.0," http://arxiv.org/abs/0912.0201.

[27] E. Sefusatti and E. Komatsu, "Bispectrum of galaxies from high-redshift galaxy surveys: primordial non-Gaussianity and nonlinear galaxy bias," *Physical Review D*, vol. 76, no. 8, Article ID 083004, 2007.

[28] L. Verde, A. F. Heavens, W. J. Percival, et al., "The 2dF galaxy redshift survey: the bias of galaxies and the density of the universe," *Monthly Notices of the Royal Astronomical Society*, vol. 335, no. 2, pp. 432–440, 2002.

[29] L. Verde and A. F. Heavens, "On the trispectrum as a Gaussian test for cosmology," *The Astrophysical Journal*, vol. 553, no. 1, pp. 14–24, 2001.

[30] W. H. Press and P. Schechter, "Formation of galaxies and clusters of galaxies by self-similar gravitational condensation," *The Astrophysical Journal*, vol. 187, pp. 425–438, 1974.

[31] S. Matarrese, L. Verde, and R. Jimenez, "The abundance of high-redshift objects as a probe of non-Gaussian initial conditions," *The Astrophysical Journal*, vol. 541, no. 1, pp. 10–24, 2000.

[32] M. Kamionkowski, L. Verde, and R. Jimenez, "The void abundance with non-gaussian primordial perturbations," *Journal of Cosmology and Astroparticle Physics*, vol. 2009, no. 1, article 010, 2009.

[33] M. Grossi, L. Verde, C. Carbone, et al., "Large-scale non-Gaussian mass function and halo bias: tests on N-body simulations," *Monthly Notices of the Royal Astronomical Society*, vol. 398, no. 1, pp. 321–332, 2009.

[34] R. K. Sheth and G. Tormen, "Large-scale bias and the peak background split," *Monthly Notices of the Royal Astronomical Society*, vol. 308, no. 1, pp. 119–126, 1999.

[35] A. Jenkins, C. S. Frenk, S. D. M. White, et al., "The mass function of dark matter haloes," *Monthly Notices of the Royal Astronomical Society*, vol. 321, no. 2, pp. 372–384, 2001.

[36] D. S. Reed, R. Bower, C. S. Frenk, A. Jenkins, and T. Theuns, "The halo mass function from the dark ages through the present day," *Monthly Notices of the Royal Astronomical Society*, vol. 374, no. 1, pp. 2–15, 2007.

[37] L. Verde, R. Jimenez, M. Kamionkowski, and S. Matarrese, "Tests for primordial non-Gaussianity," *Monthly Notices of the Royal Astronomical Society*, vol. 325, no. 1, pp. 412–418, 2001.

[38] J. Lee and S. F. Shandarin, "Comparison of analytical mass functions with numerical simulations," *The Astrophysical Journal*, vol. 517, no. 1, pp. L5–L8, 1999.

[39] B. E. Robertson, A. V. Kravtsov, J. Tinker, and A. R. Zentner, "Collapse barriers and halo abundance: testing the excursion set ansatz," *The Astrophysical Journal*, vol. 696, pp. 636–652, 2009.

[40] M. Maggiore and A. Riotto, "The halo mass function from excursion set theory. III. Non-Gaussian fluctuations," http://arxiv.org/abs/0903.1251.

[41] X. Kang, P. Norberg, and J. Silk, "Can a large-scale structure probe cosmic microwave background-constrained non-Gaussianity?" *Monthly Notices of the Royal Astronomical Society*, vol. 376, pp. 343–347, 2007.

[42] M. Grossi, K. Dolag, E. Branchini, S. Matarrese, and L. Moscardini, "Evolution of massive haloes in non-Gaussian scenarios," *Monthly Notices of the Royal Astronomical Society*, vol. 382, no. 3, pp. 1261–1267, 2007.

[43] N. Dalal, O. Dore, D. Huterer, and A. Shirokov, "Imprints of primordial non-Gaussianities on large-scale structure: scale-dependent bias and abundance of virialized objects," *Physical Review D*, vol. 77, no. 12, Article ID 123514, 2008.

[44] V. Desjacques, U. Seljak, and I. T. Iliev, "Scale-dependent bias induced by local non-Gaussianity: a comparison to N-body simulations," *Monthly Notices of the Royal Astronomical Society*, vol. 396, no. 1, pp. 85–96, 2009.

[45] A. Pillepich, C. Porciani, and O. Hahn, "Table of contents," *Monthly Notices of the Royal Astronomical Society*, p. 1959, 2009.

[46] S. Matarrese and L. Verde, "The effect of primordial non-Gaussianity on halo bias," *The Astrophysical Journal*, vol. 677, no. 2, pp. L77–L80, 2008.

[47] N. Kaiser, "On the spatial correlations of Abell clusters," *The Astrophysical Journal Letters*, vol. 284, pp. L9–L12, 1984.

[48] H. D. Politzer and M. B. Wise, "Relations between spatial correlations of rich clusters of galaxies," *The Astrophysical Journal*, vol. 285, pp. L1–L3, 1984.

[49] L. G. Jensen and A. S. Szalay, "N-point correlations for biased galaxy formation," *The Astrophysical Journal*, vol. 305, pp. L5–L9, 1986.

[50] H. J. Mo and S. D. M. White, "An analytic model for the spatial clustering of dark matter haloes," *Monthly Notices of the Royal Astronomical Society*, vol. 282, no. 2, pp. 347–361, 1996.

[51] P. Catelan, F. Lucchin, S. Matarrese, and C. Porciani, "The bias field of dark matter haloes," *Monthly Notices of the Royal Astronomical Society*, vol. 297, no. 3, pp. 692–712, 1998.

[52] G. Efstathiou, C. S. Frenk, S. D. M. White, and M. Davis, "Gravitational clustering from scale-free initial conditions," *Monthly Notices of the Royal Astronomical Society*, vol. 235, pp. 715–748, 1988.

[53] S. Cole and N. Kaiser, "Biased clustering in the cold dark matter cosmogony," *Monthly Notices of the Royal Astronomical Society*, vol. 237, pp. 1127–1146, 1989.

[54] B. Grinstein and M. B. Wise, "Non-Gaussian fluctuations and the correlations of galaxies or rich clusters of galaxies," *The Astrophysical Journal*, vol. 310, pp. 19–22, 1986.

[55] S. Matarrese, F. Lucchin, and S. A. Bonometto, "A path-integral approach to large-scale matter distribution originated by non-Gaussian fluctuations," *The Astrophysical Journal Letters*, vol. 310, no. 1, pp. L21–L26, 1986.

[56] F. Lucchin, S. Matarrese, and N. Vittorio, "Scale-invariant clustering and primordial biasing," *The Astrophysical Journal Letters*, vol. 330, pp. L21–L23, 1988.

[57] L. Verde and S. Matarrese, "Detectability of the effect of inflationary non-Gaussianity on halo bias," *The Astrophysical Journal*, vol. 706, no. 1, pp. L91–L95, 2009.

[58] A. Slosar, C. Hirata, U. Seljak, S. Ho, and N. Padmanabhan, "Constraints on local primordial non-Gaussianity from large scale structure," *Journal of Cosmology and Astroparticle Physics*, vol. 2008, no. 8, article 031, 2008.

[59] N. Afshordi and A. J. Tolley, "Primordial non-Gaussianity, statistics of collapsed objects, and the integrated Sachs-Wolfe effect," *Physical Review D*, vol. 78, no. 12, Article ID 123507, 2008.

[60] A. Cooray and R. Sheth, "Halo models of large scale structure," *Physics Report*, vol. 372, no. 1, pp. 1–129, 2002.

[61] U. Seljak, "Extracting primordial non-Gaussianity without cosmic variance," *Physical Review Letters*, vol. 102, no. 2, Article ID 021302, 2009.

[62] A. Slosar, "Optimal weighting in f_{NL} constraints from large scale structure in an idealised case," *Journal of Cosmology and Astroparticle Physics*, vol. 2009, no. 3, article 004, 2009.

[63] C. Carbone, L. Verde, and S. Matarrese, "Non-Gaussian halo bias and future galaxy surveys," *The Astrophysical Journal*, vol. 684, pp. L1–L4, 2008.

[64] C. Fedeli, L. Moscardini, and S. Matarrese, "The clustering of galaxy clusters in cosmological models with non-Gaussian initial conditions: predictions for future surveys," *Monthly Notices of the Royal Astronomical Society*, vol. 397, no. 2, pp. 1125–1137, 2009.

[65] C. Sealfon, L. Verde, and R. Jimenez, "Stacking weak-lensing signals of Sunyaev-Zel'dovich clusters to constrain cluster physics," *The Astrophysical Journal*, vol. 649, no. 1, pp. 118–128, 2006.

[66] E. Rozo, E. S. Rykoff, A. Evrard, et al., "Constraining the scatter in the mass-richness relation of maxbcg clusters with weak lensing and X-ray data," *The Astrophysical Journal*, vol. 699, no. 1, pp. 768–781, 2009.

[67] M. J. Jee, P. Rosati, H. C. Ford, et al., "Hubble space telescope weak-lensing study of the galaxy cluster xmmu j2235.3–2557 at z $\sim$ 1.4: a surprisingly massive galaxy cluster when the universe is one-third of its current age," *The Astrophysical Journal*, vol. 704, no. 1, pp. 672–686, 2009.

[68] R. Jimenez and L. Verde, "Implications for primordial non-Gaussianity (f_{NL}) from weak lensing masses of high-z galaxy clusters," *Physical Review D*, vol. 80, no. 12, Article ID 127302, 2009.

[69] D. Baumann, M. G. Jackson, P. Adshead, et al., "Probing inflation with CMB polarization," in *CMB Polarization Workshop: Theory and Foregrounds: Cmbpol Mission Concept Study*, S. Dodelson, D. Baumann, A. Cooray, J. Dunkley, and A. Fraisse, Eds., vol. 1141 of *AIP Conference Series*, pp. 10–120, 2009.

[70] E. Sefusatti, M. Liguori, A. P. S. Yadav, M. G. Jackson, and E. Pajer, "Constraining running non-Gaussianity," *Journal of Cosmology and Astroparticle Physics*, vol. 2009, no. 12, article 022, 2009.